Polyakov-quark–meson–diquark model for two-color QCD

Nils Strodthoff [a,*], Lorenz von Smekal [b,c]

[a] *Institut für Theoretische Physik, Universität Heidelberg, 69120 Heidelberg, Germany*
[b] *Institut für Kernphysik, Technische Universität Darmstadt, 64289 Darmstadt, Germany*
[c] *Institut für Theoretische Physik, Justus-Liebig-Universität Giessen, 35392 Giessen, Germany*

A R T I C L E   I N F O

A B S T R A C T

We present an update on the phase diagram of two-color QCD from a chiral effective model approach based on a quark–meson–diquark model using the Functional Renormalization Group (FRG). We discuss the impact of perturbative UV contributions, the inclusion of gauge field dynamics via a phenomenological Polyakov loop potential, and the impact of matter backcoupling on the gauge sector. The corresponding phase diagram including these effects is found to be in qualitative agreement with recent lattice investigations.

© 2014 The Authors. Published by Elsevier B.V. This is an open access article under the CC BY license (http://creativecommons.org/licenses/by/3.0/). Funded by SCOAP³.

1. Introduction

The understanding of the QCD phase diagram, in particular in regions of intermediate chemical potentials, represents an enormous theoretical challenge. The main obstacle to theoretical progress is the sign-problem in QCD [1–4]. In this situation it has become an important alternative to study finite density effects in QCD-like theories with real fermion determinants [5], as classified according to random matrix theory by the Dyson index β of their Dirac operators [6,7]. In the cases $\beta = 1$, with 2-color QCD as a representative example, and $\beta = 4$, as for QCD with quarks in the adjoint representation or QCD with the gauge group G_2 [8,9], the Dirac operator possesses an additional antiunitary symmetry, which ensures the reality or even positivity (for $\beta = 4$ with Kramers degeneracy) of the fermion determinant for a single quark flavor. In absence of such a symmetry, for $\beta = 2$ as in QCD, one is restricted to finite isospin density [10–12]. Despite the fact that such QCD-like theories differ in various important aspects from the 3-color world at finite baryon density, a better understanding of their phase diagrams can provide insight into generic features of finite density. At the same time they serve as benchmarks for quantum field-theoretical continuum methods and model descriptions. In particular, direct comparisons between functional continuum methods and lattice simulations at finite density are possible in these theories.

Two-color QCD has been studied within a number of different approaches such as chiral perturbation theory [1,6,13], ran-

dom matrix theory [7,14,15], the NJL model [16,17], and on the Lattice [18–23], see [24] for a more extensive discussion of earlier approaches. In this Letter we expand on our previous Functional Renormalization Group study of two-color QCD within the quark–meson–diquark (QMD) model [24], where the model construction and the general formalism were laid out, but where only the matter sector was taken into account in the numerical results. Here we focus on the modeling of gauge field dynamics in the form of a phenomenological Polyakov loop potential [17]. As compared to available mean-field results we thereby also include the fluctuations due to collective mesonic and baryonic excitations. At low baryon density, outside the diquark condensation phase of two-color QCD, this extension is analogous to that of the Polyakov-quark–meson model for the QCD phase diagram [25] when mesonic fluctuations are included [26–31]. With diquark condensation and diquark fluctuations, however, this will include the region of high baryon density in the phase diagram of two-color QCD and thus allow a more detailed comparison with recent lattice results [22,23].

2. Theoretical background

In this section we review the essentials of two-color QCD and its effective Polyakov-quark–meson–diquark (PQMD) model description. We furthermore introduce the necessary basics of the Functional Renormalization Group approach and the corresponding flow equations for the effective potential of the model in the leading order derivative expansion.
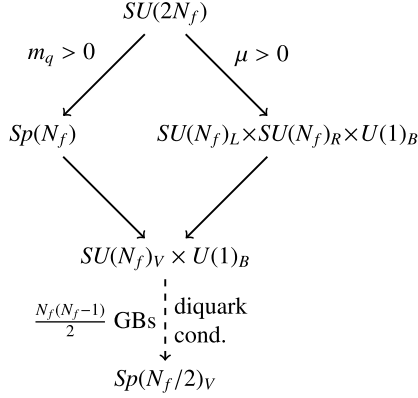
* Corresponding author.

Fig. 1. Patterns of symmetry breaking in two-color QCD with N_f flavors of fundamental quarks ($\beta = 1$).

2.1. PQMD model for two-color QCD

The key to understanding the special properties of two-color QCD is its enlarged flavor symmetry, which is in turn based on the pseudo-reality of the $SU(2)$ fundamental representation. In a theory with N_f degenerate quark flavors the enlarged flavor symmetry group is given by $SU(2N_f)$ which contains the usual flavor and baryon number $SU(N_f)_L \times SU(N_f)_R \times U(1)_B$ symmetries as subgroup. Obviously, the enlarged flavor symmetry also changes the pattern of chiral symmetry breaking; an explicitly or spontaneously generated Dirac mass term breaks the enlarged $SU(2N_f)$ to the symplectic group $Sp(N_f)$, whereas the inclusion of a chemical potential breaks it to $SU(N_f)_L \times SU(N_f)_R \times U(1)_B$. In presence of both, the residual symmetry is given by the common $SU(N_f)_V \times U(1)_B$ subgroup of the two. In the diquark condensation phase this symmetry gets broken spontaneously to $Sp(N_f/2)$ and correspondingly $N_f(N_f - 1)/2$ Goldstone bosons occur. For asymptotically large chemical potentials chiral symmetry gets (partially) restored to $Sp(N_f/2)_L \times Sp(N_f/2)_R$. It is a special property of the 2-flavor theory that this leads to a complete restoration of the chiral $SU(2)_L \times SU(2)_R$ symmetry at asymptotically large chemical potentials. The symmetry breaking patterns in two-color QCD with N_f degenerate flavors of fundamental quarks are summarized in Fig. 1.

In the following we will concentrate on the case of two flavors where the breaking $SU(4) \to Sp(2)$ is locally the same as the simple vector-like breaking of $SO(6) \to SO(5)$. The corresponding five (pseudo-)Goldstone bosons are identified with the three pions plus a scalar bosonic diquark/antidiquark pair, which is thus degenerate with the pions at vanishing chemical potential. These diquarks play a dual role as pseudo-Goldstone bosons and as the lightest baryonic degrees of freedom in the theory. In this case, diquark condensation simply corresponds to $SU(2)_V \times U(1)_B \to Sp(1)_V \simeq SU(2)_V$, i.e. to the spontaneous breaking of the $U(1)_B$ for baryon number conservation. Most importantly, the pattern of symmetry breaking is correctly reproduced in a quark–meson–diquark model, as an effective model of quarks, mesons and diquarks.

In the case of two quark flavors it is described by the (Euclidean) Lagrangian [24]

$$\mathcal{L}_{\mathrm{PQMD}} = \bar{\psi}\big(\slashed{D} + h(\sigma + i\gamma^5 \vec{\pi}\vec{\tau}) - \mu\gamma^0\big)\psi$$
$$+ \frac{h}{2}\big(\Delta^*(\psi^T C i\gamma^5 \tau_2 T_2 \psi) + \Delta(\psi^\dagger C i\gamma^5 \tau_2 T_2 \psi^*)\big)$$
$$+ \frac{1}{2}(\partial_\mu \sigma)^2 + \frac{1}{2}(\partial_\mu \vec{\pi})^2 + V(\vec{\phi})$$
$$+ \frac{1}{2}(\partial_\mu - 2\mu\delta_{\mu 0})\Delta\big(\partial^\mu + 2\mu\delta_0^\mu\big)\Delta^* + \mathcal{U}_{\mathrm{Pol}}, \qquad (1)$$

with Yukawa coupling h, and τ_i denoting Pauli matrices in flavor space; $T_i = \frac{\sigma_i}{2}$ are the $SU(2)$ color generators and $C = \gamma^2\gamma^0$ is the charge conjugation matrix in spinor space. We furthermore define the vector $\vec{\phi} = (\sigma, \vec{\pi}, \mathrm{Re}\,\Delta, \mathrm{Im}\,\Delta)$ of meson and diquark fields which transforms as a vector under the enlarged $O(6) \simeq SU(4)$ flavor symmetry. The color covariant derivative is given by $D_\mu = \partial_\mu + iA_\mu$ with a constant background gauge field $A_\mu = \delta_{\mu 0}A_0$ in the Polyakov gauge, i.e. for $SU(2)$ simply with $A_0 = T^3 a_0$. The Polyakov loop whose thermal expectation value serves as an order parameter for confinement in the pure gauge theory is thus represented as

$$\Phi \equiv \frac{1}{2}\,\mathrm{tr}_c\, e^{i\beta A_0} = \cos\left(\frac{\beta a_0}{2}\right). \qquad (2)$$

While one could employ Polyakov loop potentials from lattice simulations or functional continuum methods [31] in the future, here we present results for a phenomenological Polyakov loop potential [17] of the form

$$\mathcal{U}_{\mathrm{Pol}}(\Phi; T, T_0) = -bT\big[24\Phi^2 e^{-a/T} + \log(1 - \Phi^2)\big], \qquad (3)$$

which is a 2-color variant of the commonly used 3-color logarithmic Polyakov loop potential [32,33]. The deconfinement transition itself is fixed by the parameter a which is related to the critical temperature T_0 of the pure gauge theory as $a = T_0 \log 24$, whereas a strong coupling expansion relates b to the string tension $\sqrt{\sigma}$ via $b = (\sigma/a)^3$. The parameter b determines the mixing between chiral and deconfinement transition and can be used to adjust the pseudo-critical temperature for the chiral transition relative to the deconfinement transition. It is typically chosen such that the two crossovers coincide [32]. Here we simply fix $b = (\sigma/a)^3$ and adjust T_0 with N_f and μ as described below. The rational for this adjustment is to account for the implicit feedback of the matter sector on the gluodynamics and hence the Polyakov loop potential [25]. This includes sea quark effects on the gluonic correlations, for example, in contradistinction to the valence quark contributions as here described explicitly by the fermionic flow.

The critical temperatures of pure $SU(N_c)$ gauge theories have been well-investigated on the lattice, see [34] and the references therein. In units of the string tension they are very well described by the corresponding value in the large N_c limit plus a $1/N_c^2$ correction term, all the way down to $N_c = 2$ [35]. For $SU(2)$ this yields $T_c/\sqrt{\sigma} = 0.7092(36)$ [34] which corresponds to $T_c = 312$ MeV in physical units assuming a string tension with $\sqrt{\sigma} = 440$ MeV. This fixes $T_0(N_f = 0, \mu = 0) = T_c$.

We may generally relate couplings α_T and α_0 at sufficiently close-by temperature scales T and T_0 assuming a logarithmic dependence [36] of the form

$$\ln\left(\frac{T}{T_0}\right) = a\left(\frac{\alpha_0}{\alpha_T} - 1\right) \qquad (4)$$

with some nonperturbative coefficient a which depends on N_f and N_c (for $N_f = 0$ of the order $1/N_c$). In order to include Debye screening effects we consider the *effective charge* $\alpha_{\mathrm{eff}}(p)$ in the plasma [37] at the soft scale $p \sim gT$ as in [25],

$$\alpha_{\mathrm{eff}}(gT) = \frac{\alpha_T}{1 + b(\mu/T)}, \qquad (5)$$

where $b(\mu/T) \equiv m_D^2/(gT)^2$ is given by the Debye mass m_D per $p \sim gT$. At one-loop level it would be [37]

$$b\left(\frac{\mu}{T}\right) = \frac{N_c}{3} + \frac{N_f}{12}\left(1 + \frac{3}{\pi^2}\frac{\mu^2}{T^2}\right). \qquad (6)$$

The Debye mass increases with μ and hence the effective charge decreases. The simplest way to include Debye screening thus is to

consider lines $T(\mu)$ at constant α_{eff}, with $T_0 \equiv T(0)$, $b_0 \equiv b(0)$ and (4) these are obtained as,

$$\ln\left(\frac{T(\mu)}{T_0}\right) = \frac{b_0 - b(\mu/T)}{1 + b(\mu/T)}a, \tag{7}$$

where a is the N_c- and N_f-dependent but μ-independent nonperturbative coefficient from Eq. (4). If we expand

$$b\left(\frac{\mu}{T}\right) = b_0 + b_1\frac{\mu^2}{T^2} + \cdots \tag{8}$$

the leading logarithmic behavior of $T(\mu)$ near $\mu = 0$ becomes

$$\ln\left(\frac{T(\mu)}{T_0}\right) = -\frac{ab_1}{1 + b_0}\frac{\mu^2}{T_0^2}. \tag{9}$$

We can test this simple argument with the critical temperatures of the pure $SU(N_c)$ gauge theories: Using $N_f = 0$, $\alpha \sim 1/N_c$ and $b \sim N_c$ in the large N_c limit, one concludes that the effective charge decreases as $1/N_c^2$. Because the number of gluons grows with N_c^2, the assumption that $N_c^2\alpha_{\text{eff}} = \text{const.}$ in this case, together with $a \sim 1/N_c$ in (4), yields

$$\ln\left(\frac{T_c(N_c)}{T_c^\infty}\right) = \frac{c}{N_c^2}, \tag{10}$$

with some constant c. Fitting the lattice data for $N_c = 2, \ldots, 8$ as collected in [34] to this two parameter form works quite well. For comparison, we obtain with this form $T_c^\infty/\sqrt{\sigma} = 0.5962(16)$ with a reasonable $\chi^2/\text{d.o.f.} = 1.27$, as compared to

$$\frac{T_c}{\sqrt{\sigma}} = 0.5949(17) + \frac{0.458(18)}{N_c^2}, \tag{11}$$

from [34] with $\chi^2/\text{d.o.f.} = 1.18$. If we exclude the $N_c = 2$ value for not being close enough to the large N_c limit, we obtain $T_c^\infty/\sqrt{\sigma} = 0.5952(24)$ and our fit with (10) is practically indistinguishable from (11) of Ref. [34] for $N_c \geqslant 3$. It is thus consistent with general large-N_c arguments at this order [38].

An analogous argument also applies when varying the number of flavors N_f. In order to model the density dependence of Debye screening we therefore simply replace the parameter T_0 in the Polyakov loop potential (3) by the line $T_0(N_f, \mu)$ of constant effective charge with $T_0(0, 0) = T_c = 312$ MeV (for $N_c = 2$ here). From (9) at the leading order in μ^2/T_c^2 this line will hence be of the form, with new constants a and b,

$$T_0(N_f, \mu) = T_c \exp\left(-aN_f\left(1 + b\frac{\mu^2}{T_c^2}\right)\right). \tag{12}$$

The non-perturbative coefficient a herein should first be fixed such that the deconfinement temperature at vanishing chemical potential matches (suitably extrapolated) lattice results. Since $SU(2)$ simulations with comparably light dynamical quarks are phenomenologically less relevant than those of real QCD thermodynamics, they have received less attention and results are therefore rather limited. As an orientation we use the value for the deconfinement crossover temperature of around 217 MeV obtained from simulations with two degenerate flavors of dynamical Wilson quarks [22,23], albeit with masses considerably above their physical counterparts in QCD. Because the transition temperature is expected to further decrease with decreasing quark masses, we employed a value of $a = 0.19$ corresponding to $T_0(2, 0) = 212$ MeV which will then lead to a deconfinement crossover temperature of around 200 MeV.

A reasonable way to fix the second non-perturbative coefficient b in Eq. (12) would be to match the curvature of the pseudo-critical line extracted from the lattice a posteriori. Again due to

a lack of suitably accurate lattice data for two-color QCD we have only investigated the impact of different parameter values for b in a more exploratory fashion for now. In the following section we will simply compare results with $b = 0$, $b = 2.6$ and $b = 5.2$ to exemplify the impact of Debye screening in the unquenching effects from the matter sector on the deconfinement transition at finite density.

2.2. Functional Renormalization Group

The Functional Renormalization Group is a powerful nonperturbative tool for calculations in quantum field theory and statistical physics. Here we employ the approach pioneered by Wetterich [39] with a so-called effective average action as the central object, see [40–45] for general introductions. The FRG aims at computing the full quantum effective action by relating a classical or microscopic bare action at the ultraviolet cutoff scale Λ to the corresponding average action at some lower scale k, the scale-dependent analogue of the effective action. This RG scale k introduced by an infrared regulator is then successively lowered which yields the evolution of the scale-dependent effective average action with the RG scale k or, correspondingly, with $t = \log k/\Lambda$ as described by the exact flow equation

$$\partial_t \Gamma_k = \frac{1}{2}\text{STr}\left\{\left[\Gamma_k^{(2)} + R_k\right]^{-1}\partial_t R_k\right\}, \tag{13}$$

which assumes the form of a 1-loop equation, however, involving full (scale- and field-dependent) propagators. Here $\Gamma^{(2)}$ denotes the second functional derivative of the effective average action with respect to the fields and the supertrace involves a trace both over momentum space and internal indices and includes an additional minus sign in the fermionic subsector. As the flow equation (13) can rarely be solved exactly truncations are required. Here we employ the leading order derivative expansion in which only a scale-dependent effective potential is taken into account. Thus the Ansatz for the effective average action simply reads, in terms of the Lagrangian (1),

$$\Gamma_k = \int d^4x\, \mathcal{L}_{\text{PQMD}}\big|_{V(\phi)\to U_k(\rho^2, d^2)-c\sigma}, \tag{14}$$

where $\rho^2 = \sigma^2 + \vec{\pi}^2$ and $d^2 = \Delta^*\Delta$ denote the two $SU(2) \times U(1)_B$ invariants and the $c\sigma$ term represents an explicit breaking, which is taken into account at the end of the flow. It is crucial to consider an Ansatz for the scale-dependent effective potential U_k which is a genuine function of the two independent invariants ρ^2 and d^2 as the potential at finite chemical potential is only required to be consistent with the reduced symmetry $SU(2) \times U(1)_B$ instead of the full enlarged flavor $SU(4)$ at vanishing chemical potential. This Ansatz is consistent with the full $SU(4)$ symmetry at $\mu = 0$ as one can recast it as a function of a single variable $\phi^2 = \rho^2 + d^2$ again. Employing 3-dimensional analogues of the LPA-optimized regulator functions [46] which are commonly used in finite-temperature applications [47], $R_{k,B} = (k^2 - \vec{p}^2)\Theta(k^2 - \vec{p}^2)$ and $R_{k,F} = i\vec{p}(-1 + k/|\vec{p}|)\Theta(k^2 - \vec{p}^2)$, for bosonic and fermionic fields respectively, the flow equation for the effective potential takes the form [24]

$$\partial_t U_k = \frac{k^5}{12\pi^2}\left\{\frac{3}{E_k^\pi}\left(1 + 2n_b(E_k^\pi; T)\right)\right.$$
$$+ \sum_{i=1}^3 \frac{3z_i^4 - \alpha_1 z_i^2 + \alpha_0}{(z_{i+1}^2 - z_i^2)(z_{i+2}^2 - z_i^2)}\frac{1}{z_i}\left(1 + 2n_b(z_i; T)\right)$$
$$\left. - \sum_\pm \frac{8}{E_k^\pm}\left(1 \pm \frac{\mu}{\epsilon_k}\right)\left(1 - 2n_q(E_k^\pm; T, \Phi)\right)\right\}, \tag{15}$$

where $E_k^\pi = \sqrt{k^2 + 2\partial U_k/\partial \rho^2}$, $E_k^\pm = \sqrt{h^2 d^2 + (\epsilon_k \pm \mu)^2}$ and $\epsilon_k = \sqrt{k^2 + h^2 \rho^2}$. The quantities z_i in the sigma-diquark sector denote the roots of a cubic polynomial in $p_0^2 = -z^2$ with coefficients β_i. These together with the coefficients α_i of the corresponding quadratic polynomial in the numerator are listed explicitly in [5,24]. They all depend on the renormalization scale, the field invariants ρ^2 and d^2, on the chemical potential and the derivatives of the scale-dependent effective potential. The Polyakov loop enhanced fermion occupation numbers are given by

$$n_q(E; T, \Phi) = \frac{1 + \Phi e^{E/T}}{1 + 2\Phi e^{E/T} + e^{2E/T}}. \tag{16}$$

and reduce to the usual Fermi–Dirac distribution for $\Phi = 1$, whereas $n_b(E; T) = 1/(\exp(E/T) - 1)$ denotes the Bose–Einstein distribution function.

In our approach the gauge field a_0 is treated as a background field. The integration of Eq. (15) yields an effective potential as function of ρ^2, d^2 and a_0 which is then minimized with respect to all three variables to obtain chiral and diquark condensates and the expectation value of the Polyakov variable Φ as a function of temperature and chemical potential.

In numerical calculations it is of course important to remember the range of validity of the approach. For a given UV cutoff Λ the assumption of a temperature- and chemical-potential-independent bare action in the UV, for example, severely restricts the accessible range of temperatures and/or chemical potentials. This is most easily seen in the case of finite temperature where the flow starts to deviate from the vacuum flow only at around $k \approx 2\pi T$. This restricts the allowed temperature range at a fixed UV cutoff to values below $T \sim \Lambda/(2\pi)$. The only way of enlarging this range is to augment the model result with the expected perturbative behavior, which then also ensures thermodynamic consistency. In fact one may understand these additional perturbative UV contributions as being necessary to describe the thermodynamics of the microscopic model at the UV cutoff scale. To achieve this one can integrate the purely thermal flow, i.e. the difference between finite temperature and vacuum flow, from the UV cutoff scale Λ to infinity. The result is then added to the UV potential before integrating the flow equation (15). Obviously this gives rise to temperature- and chemical-potential-dependent initial conditions in the UV. Note that such a procedure can in general not merely modify the thermodynamics but affect the phase structure itself. Here we implement this improvement only in the fermionic fluctuations for which the purely thermal flow reads,

$$\partial_t U_k^{(T,\mu)} - \partial_t U_k^{(T=0,\mu)}$$
$$= \frac{k^5}{3\pi^2} \sum_\pm \frac{4}{E_k^\pm} \left(1 \pm \frac{\mu}{\epsilon_k} \right) n_q(E_k^\pm; T, \Phi), \tag{17}$$

see also [47] for a discussion of purely thermal flows. As compared to previous studies [27,28,48], which included analogous but field-independent UV contributions to ensure a proper Stefan–Boltzmann limit, we include the full field dependence here. A particular simplification in the fermionic sector thereby is that the right hand side of the corresponding flow is independent of the effective potential and can be straightforwardly integrated.

2.3. Numerical procedure

For a fixed value a_0 of the background gauge field the flow equation (15) for the effective potential was solved on a two-dimensional grid in field space as in Ref. [24] thereby retaining the full field dependence of the equation. As the gauge field is treated simply as a background field in our approach, the full
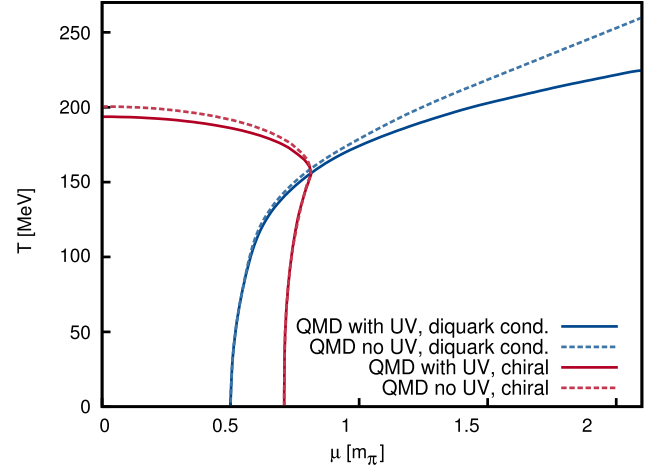

Fig. 2. Comparison of FRG results for the QMD model phase diagram with and without the thermal UV contributions (17) to the fermionic flow. Chiral crossover lines (half-value of the chiral condensate) are depicted in red, the second order phase boundary of the diquark condensation phase found at small temperatures and large chemical potentials in blue. (For interpretation of the references to color in this figure legend, the reader is referred to the web version of this article.)

three-dimensional effective potential as a function of the invariants ρ^2, d^2 and a_0 in the IR is obtained by combining results from runs with different values of a_0. In this way one obtains a discretized IR potential which can be interpolated for example using cubic splines and which is subsequently minimized. Not only does this provides a very efficient way of minimizing the full two-dimensional effective potential in the infrared, using relatively few of the expensive evaluations of the flow equation, but it also allows to conveniently extract its derivatives at the minimum which can then be used to define crossover criteria as discussed below.

3. Results

3.1. Impact of thermal UV contributions

The effect of the perturbative UV contributions discussed in the previous section is seen in Fig. 2 where we compare the full FRG result for the QMD model phase diagram with these thermal UV contributions from (17) to the corresponding result of Ref. [24] without them. The phase diagram shows a phase of broken chiral symmetry at small temperatures and chemical potentials whereas for large chemical potentials one finds a diquark condensation phase signaled by a nonvanishing diquark condensate, see [24] for a more detailed discussion of the QMD model phase diagram. The inclusion of UV contributions leads to a slight suppression of the chiral condensate at larger temperatures which consequently shifts the chiral crossover line to somewhat lower temperatures. A similar effect is observed for values of the chemical potential μ above the onset of diquark condensation at half the pion mass m_π. The boundary of the diquark condensation phase gets pushed towards lower temperatures more and more as μ is further increased. It is important to note, however, that in contrast to corresponding mean-field calculations [24], for which the inclusion of the full thermal contributions lead to the appearance of a tricritical point along the diquark condensation phase boundary, with fluctuations this boundary remains to be of second order throughout the entire parameter range investigated here.

3.2. Vanishing chemical potential and crossover criteria

We start our discussion of the PQMD model results with the case of vanishing chemical potential where the effective potential
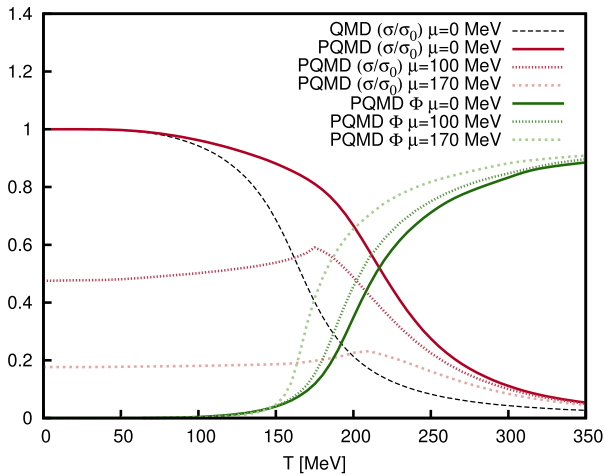
Fig. 3. Chiral condensate (PQMD and QMD model) and Polyakov loop as function of temperature for vanishing and non-vanishing chemical potential.

Fig. 4. PQMD model at $\mu = 0$: Comparison of crossover criteria.

is still required to show the full enlarged $SU(4) \simeq SO(6)$ symmetry and hence the calculation with the $O(6)$ symmetric effective potential coincides with the full solution. In [24] it was verified by an analysis of the critical exponents that the finite temperature transition was consistent with the expected $O(6)$ universality class corresponding to a symmetry breaking pattern $SU(4) \rightarrow Sp(2)$ or isomorphically $SO(6) \rightarrow SO(5)$. This will still hold in the present case since the critical physics is governed by the bosonic matter sector, at least as long as the Polyakov loop is taken as a background (mean-)field without dynamical matter feedback on gauge field fluctuations.

Fig. 3 shows the temperature dependence of the chiral condensate and the Polyakov loop as quasi-order parameters for the chiral and deconfinement transitions. For comparison we also include the chiral condensate obtained from a pure QMD model calculation corresponding to a fixed value of $a_0 = 0$. At this point the main effect of the Polyakov loop on the chiral condensate is to shift the chiral transition to larger temperatures. As both the chiral and the deconfinement transition turn into crossovers for finite quark masses, the corresponding transition temperatures are not uniquely defined. We therefore compare up to three different definitions and use the resulting variations as indications for the widths of the two crossovers. The simplest one is the point where the order parameter reaches half of its value at $T = \mu = 0$. While this does not even define a proper pseudo-critical temperature, it turns out to be a useful measure for chiral restoration in the diquark condensation region, as discussed in Section 3.4, where there is no pseudo-critical line. A second commonly used definition is the inflection point of the order parameter along the temperature axis, i.e. the extremum of its temperature derivative which is readily computable, in principle. This can become increasingly difficult, however, in regions where the slope of the order parameter is nearly constant, and it fails entirely of course when there is no inflection point as for the chiral condensate in the diquark condensation region for $\mu > m_\pi / 2$, cf. Fig. 3. Finally as a third criterion we use the maxima of the corresponding susceptibilities, i.e. the chiral and the Polyakov loop susceptibility, which are easily accessible by taking the appropriate second derivatives of the effective potential with respect to the order parameters. The maxima of the susceptibilities define proper pseudo-critical lines [49] and are thus the probably most natural choices from the point of view of critical phenomena.

The corresponding temperature derivatives and susceptibilities are shown in Fig. 4 and the associated crossover temperatures are compiled in Table 1. These values should not be taken
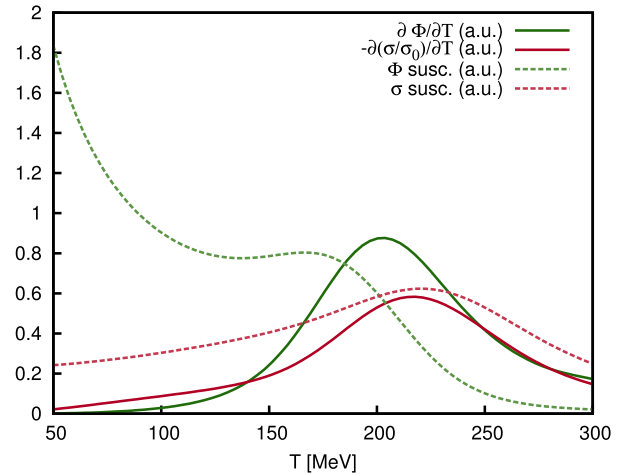
too literally as quantitative predictions because they show some sensitivity to the parameters, especially to the adjusted sigma mass. As mentioned above, the deconfinement crossover temperature from the inflection point is somewhat below the central value but still within errors of the corresponding lattice result of 217(23) MeV [22], which was obtained from simulations with considerably larger quark masses, however.

Table 1

Chiral and deconfinement crossover temperatures at $\mu = 0$ for pion decay constant $f_\pi = 76$ MeV, a physical pion mass $m_\pi = 138$ MeV defined via the onset of the onset at vanishing temperature and a sigma (screening-)mass of 551 MeV.

Criterion	T_c^{chiral} [MeV]	$T_c^{\text{deconf.}}$ [MeV]
Half-value	219.1	214.4
Inflection pt.	213.0	198.2
Susceptibility	221.1	185.5

3.3. $O(6)$ symmetric effective potential

In this subsection we address the calculation with an $O(6)$ symmetric effective potential depending on the single invariant $\phi^2 = \rho^2 + d^2$. For $\mu = 0$ the solution coincides with the full solution, but it will deviate from that at finite μ. Nevertheless, it represents a good approximation to the full solution at least for small chemical potentials where the $O(6)$ symmetry still holds approximately. As discussed in [24] this calculation closely resembles the corresponding Polyakov-quark–meson model calculations for 3-color QCD [26–30]. On one hand, the only difference in the chiral sector is the a larger number of would-be Goldstone bosons, five here instead of the three pions for the case of two light flavors in QCD, see [6] for a discussion of the Goldstone spectrum. Two of these five pseudo-Goldstone bosons couple to the chemical potential in a way analogous to the coupling of charged pions to an isospin chemical potential QCD, see [12] for a detailed discussion of the relation between two-color QCD at finite baryon density and QCD at finite isospin density. On the other hand the gauge sectors in the two theories are of course fundamentally different. Despite these differences the corresponding phase diagrams turn out to share the same qualitative behavior.

Two phase diagrams obtained from calculations with $O(6)$-symmetric effective potential are shown for comparison in Figs. 5 and 6. In Fig. 5 we have used a constant $T_0 = 212$ MeV in the Polyakov loop potential, while Fig. 6 shows the corresponding result with the chemical-potential-dependent $T_0(\mu) = T_0 \exp\{-c\mu^2/T_0^2\}$ and $c = 0.46$ corresponding to $b = 2.6$ in Eq. (12)
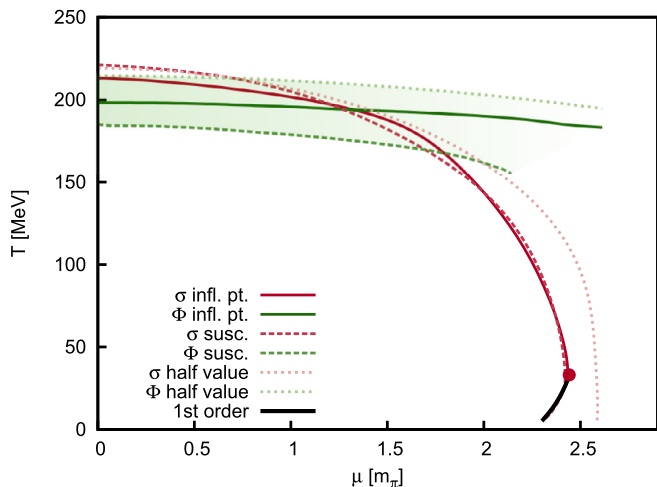
Fig. 5. PQMD model phase diagram for an $O(6)$ symmetric effective potential and constant T_0. Chiral crossover lines are depicted in red, deconfinement crossover lines in green for three different crossover criteria, cf. the discussion in Section 3.2, and first order transitions in solid black. (For interpretation of the references to color in this figure legend, the reader is referred to the web version of this article.)

Fig. 6. PQMD model phase diagram for an $O(6)$ symmetric effective potential and $T_0 = T_0(\mu)$ ($b = 2.60$). Color coding as in Fig. 5.

to model the leading finite density effects from Debye screening via the assumption of constant effective charge along the transition line in the pure glue potential as discussed in Section 2.1. In the first case the deconfinement temperature only shows a very slight decrease with increasing chemical potential. The three different definitions are used to visualize the width of the deconfinement crossover. In the second case one observes a considerable decrease of the deconfinement crossover temperature with chemical potential. At the same time, as one can infer directly from Fig. 3 and indirectly from the focusing of the deconfinement crossover lines corresponding to different crossover criteria, the crossover becomes increasingly rapid with increasing chemical potential but remains a continuous transition throughout. The corresponding chiral crossover lines remain more or less parallel to the deconfinement transition up to a temperature of around 80 MeV from where on the chiral transition bends downwards and eventually merges into the critical endpoint, whereas the deconfinement crossover continues to decrease approximately linearly with the chemical potential until it starts bending away from the $T = 0$ axis. Apart from this splitting of the two transitions near the critical endpoint, which was not observed in the analogous 3-color calculations, these phase diagrams agree qualitatively with the corresponding PQM model results for QCD [29,30]. In particular, the density-dependent transition temperature $T_0(\mu)$ in the Polyakov loop potential has the same overall effect in either case. Moreover, the phase diagrams in Figs. 5 and 6 both show quarkyonic phases of confined but chirally restored matter although their sizes differ considerably. One should keep in mind, however, that both phase diagrams yield equally inappropriate descriptions of two-color QCD at finite baryon density as we have so far neglected the diquarks as the baryonic degrees of freedom in this theory.

3.4. Full effective potential

The correct inclusion of the diquark degrees of freedom is addressed in the present subsection where we discuss the full solution of the PQMD model flow equation for the effective potential. Again we compare the phase structure for a constant T_0 in Fig. 7(a) to that with the chemical-potential-dependent $T_0 = T_0(\mu)$ in Fig. 7(b) and Fig. 7(c). The parameters are the same as in the previous subsection. Similar to our observation there, without the density dependence from the Debye mass in the pure glue po-
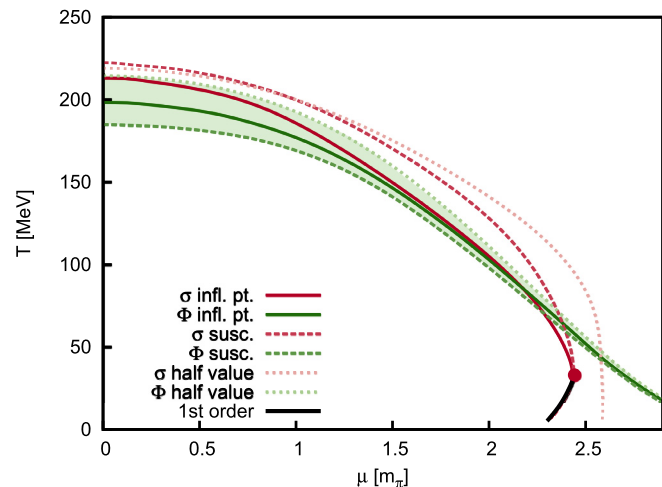
tential, the deconfinement crossover is almost independent of the chemical potential here as well. This is fully in line with previous PNJL model mean-field results for constant T_0 [17].

The lines from inflection points and susceptibility peaks for the chiral transition (not shown here) both stay above the diquark condensation phase boundary and lose their meaning as pseudo-critical lines at large chemical potentials. That is why we only show the half-value line as a representative contour line to indicate chiral symmetry restoration, in particular inside the diquark condensation phase where it is related to the analogue of the BEC–BCS crossover in two-color QCD.

Very similar to the results from the previous section the inclusion of matter backcoupling on the gauge sector, such as the density-dependent Debye screening, lead to a decrease of the deconfinement crossover temperature with increasing chemical potential in Fig. 7(b) and Fig. 7(c). As a result, the deconfinement transition traverses deep into the diquark condensation phase leading to a phase diagram which is in overall good qualitative agreement with recent lattice results [23,22]. The comparison between Fig. 7(b) and Fig. 7(c) serves to illustrate the impact of the non-perturbative coefficient b. As expected, increasing b leads to a stronger decrease of the deconfinement crossover temperature with increasing chemical potential. This comes together with a certain suppression of the diquark condensation transition temperature above their intersection point. The shape of the diquark condensation phase tends to become more rectangular, which would be in quite good agreement with most recent lattice results [23].

On a more quantitative level, however, these lattice results indicate that the practically μ-independent horizontal boundary of the diquark condensation phase occurs at a temperature which is only about half of that of the deconfinement transition at $\mu = 0$ [23]. This might at least partially be explained by the rather heavy quark masses there, which should be further investigated, but at the moment it is nevertheless at odds with the available model results.

Disregarding the differences in physical parameters between the lattice simulations and the FRG calculation, the deconfinement crossover in the lattice simulations still shows a somewhat sharper decrease with chemical potential as compared to the FRG calculation. This might hint at effects of matter backcoupling on the gauge sector at large chemical potentials which are beyond the expansion in (8) for the leading order μ^2-dependence in $T_0(\mu)$ from the density-dependence of the Debye mass. Furthermore, previous 4-flavor lattice simulations [20] have provided evidence of
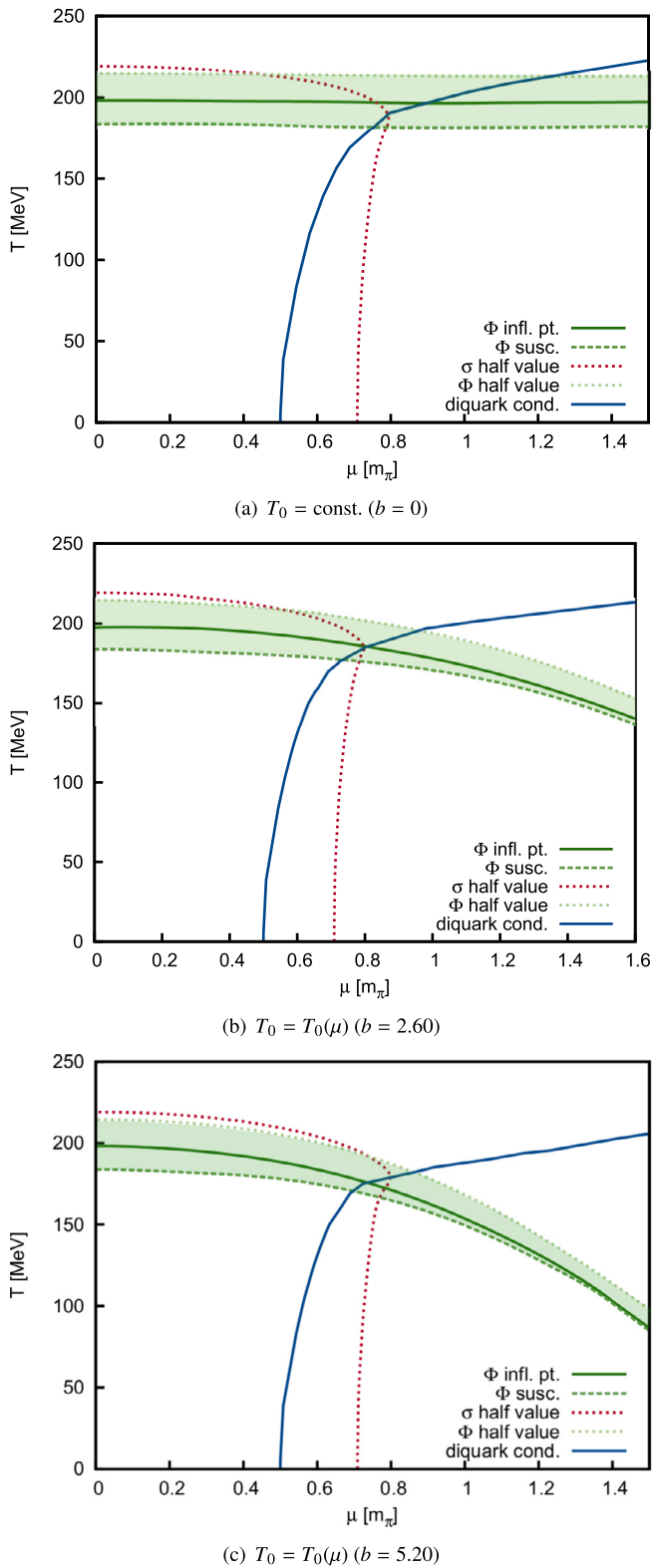
(a) $T_0 = \text{const.}$ ($b = 0$)

(b) $T_0 = T_0(\mu)$ ($b = 2.60$)

(c) $T_0 = T_0(\mu)$ ($b = 5.20$)

Fig. 7. PQMD model phase diagrams illustrating the effects of matter-backcoupling using different parameter values for b, see Eq. (12). Chiral crossover lines (half-value of the condensate) are depicted in red, deconfinement crossover lines in green (comparing three different crossover criteria) and the second order phase boundary of the diquark condensation phase in blue. (For interpretation of the references to color in this figure legend, the reader is referred to the web version of this article.)

a first order finite temperature phase transition at large chemical potentials implying the existence of a tricritical point along the diquark condensation phase boundary which was attributed to light mesonic/diquark fluctuations [20]. While this will certainly depend on the number of flavors, the fact that it is not observed in our 2-flavor FRG calculations here, although the latter includes the relevant fluctuations, points to insufficiencies at large chemical potentials which might be resolved by considering chemical-potential-dependent initial conditions. More generally, from a QCD perspective one should take into account the temperature and chemical potential dependence of the two-gluon exchange diagrams which drive the flow of 4-Fermi interactions at large scales. The difference of the vacuum contribution and the corresponding contributions at finite temperature and chemical potential translate after bosonization into temperature- and chemical-potential-dependent contributions to the UV potential.

At some point, however, a proper inclusion of gauge degrees of freedom beyond the simple coupling to a phenomenological Polyakov loop potential becomes indispensable. In a functional approach such a description of two-color QCD could be achieved quite analogously to what has been done in the case of three colors [50] already.

4. Summary and conclusions

In this Letter we presented first results on the phase diagram of two-color QCD from a QMD model calculation on the one hand extending earlier results [24] by the inclusion of gauge degrees of freedom in the form a coupling to phenomenological Polyakov loop potential, and on the other hand extending earlier mean-field calculation [17] by the inclusion of collective mesonic and baryonic excitations and effects of matter-backcoupling on the gauge sector. Furthermore the results presented here include additional UV contributions ensuring thermodynamic consistency which are particularly important in regions of the phase diagram where the temperature is large compared to the UV cutoff scale. These lead to a certain decrease of both, the chiral and the diquark-condensation transition temperatures.

Similar to the 3-color case [25,26], the matter backcoupling onto the gauge sector, here implemented via a chemical-potential-dependent temperature $T_0(\mu)$ entering the Polyakov loop potential, turns out to be crucial for the 2-color case as well. Whereas the deconfinement transition temperature stays practically independent of the chemical potential for constant T_0, similar to what has been observed in a PNJL model analysis [17], the matter backcoupling leads to a significant decrease of the transition temperature with increasing chemical potential. The corresponding phase diagram is found to be in good qualitative agreement with recent lattice results.

It would provide interesting insights to study the PQMD model in an extended truncation which goes beyond the zeroth order in the derivative expansion and which is fully consistent with the reduced symmetry of the theory at vanishing chemical potential, although this is expected to lead only to quantitative changes of the phase diagram. The resolution of the remaining discrepancies discussed in the previous section will be important for our general understanding of the reliability of FRG results at large chemical potentials and might in this sense also be directly relevant for the corresponding 3-color calculations. Further input might come from the comparison of two-color QCD thermodynamics between lattice results and functional methods. In this respect we look forward to further lattice results for two-color QCD with $N_f = 2$ quark flavors which can be most easily treated in the effective model and functional renormalization group approaches as discussed here.

Acknowledgements

References

[1] J. Kogut, M.A. Stephanov, D. Toublan, Phys. Lett. B 464 (1999) 183, arXiv:hep-ph/9906346.
[2] K. Splittorff, D. Son, M.A. Stephanov, Phys. Rev. D 64 (2001) 016003, arXiv:hep-ph/0012274.
[3] P. de Forcrand, PoS LAT2009 (2009) 010, arXiv:1005.0539.
[4] G. Aarts, PoS LATTICE2012 (2012) 017, arXiv:1302.3028.
[5] L. von Smekal, Nucl. Phys. B, Proc. Suppl. 228 (2012) 179, arXiv:1205.4205.
[6] J. Kogut, et al., Nucl. Phys. B 582 (2000) 477, arXiv:hep-ph/0001171.
[7] T. Kanazawa, T. Wettig, N. Yamamoto, J. High Energy Phys. 1112 (2011) 007, arXiv:1110.5858.
[8] K. Holland, et al., Nucl. Phys. B 668 (2003) 207, arXiv:hep-lat/0302023.
[9] A. Maas, et al., Phys. Rev. D 86 (2012) 111901, arXiv:1203.5653.
[10] D. Son, M.A. Stephanov, Phys. Rev. Lett. 86 (2001) 592, arXiv:hep-ph/0005225.
[11] J. Kogut, D. Sinclair, Phys. Rev. D 70 (2004) 094501, arXiv:hep-lat/0407027.
[12] K. Kamikado, et al., Phys. Lett. B 718 (2013) 1044, arXiv:1207.0400.
[13] K. Splittorff, D. Toublan, J. Verbaarschot, Nucl. Phys. B 620 (2002) 290, arXiv:hep-ph/0108040.
[14] B. Vanderheyden, A. Jackson, Phys. Rev. D 64 (2001) 074016, arXiv:hep-ph/0102064.
[15] B. Klein, D. Toublan, J. Verbaarschot, Phys. Rev. D 72 (2005) 015007, arXiv:hep-ph/0405180.
[16] C. Ratti, W. Weise, Phys. Rev. D 70 (2004) 054013, arXiv:hep-ph/0406159.
[17] T. Brauner, K. Fukushima, Y. Hidaka, Phys. Rev. D 80 (2009) 074035, arXiv:0907.4905.
[18] S. Hands, et al., Eur. Phys. J. C 17 (2000) 285, arXiv:hep-lat/0006018.
[19] J. Kogut, et al., Phys. Rev. D 64 (2001) 094505, arXiv:hep-lat/0105026.
[20] J.B. Kogut, D. Toublan, D. Sinclair, Phys. Lett. B 514 (2001) 77, arXiv:hep-lat/0104010.
[21] S. Hands, S. Kim, J.I. Skullerud, Eur. Phys. J. C 48 (2006) 193, arXiv:hep-lat/0604004.
[22] S. Cotter, et al., Phys. Rev. D 87 (2013) 034507, arXiv:1210.4496.
[23] T. Boz, et al., Eur. Phys. J. A 49 (2013) 87, arXiv:1303.3223.
[24] N. Strodthoff, B.J. Schaefer, L. von Smekal, Phys. Rev. D 85 (2012) 074007, arXiv:1112.5401.
[25] B.J. Schaefer, J.M. Pawlowski, J. Wambach, Phys. Rev. D 76 (2007) 074023, arXiv:0704.3234.
[26] T.K. Herbst, J.M. Pawlowski, B.J. Schaefer, Phys. Lett. B 696 (2011) 58, arXiv:1008.0081.
[27] V. Skokov, B. Friman, K. Redlich, Phys. Rev. C 83 (2011) 054904, arXiv:1008.4570.
[28] V. Skokov, et al., Phys. Rev. C 82 (2010) 015206, arXiv:1004.2665.
[29] T.K. Herbst, J.M. Pawlowski, B.J. Schaefer, Acta Phys. Pol. B, Proc. Suppl. 5 (2012) 733, arXiv:1202.0758.
[30] T.K. Herbst, J.M. Pawlowski, B.J. Schaefer, Phys. Rev. D 88 (2013) 014007, arXiv:1302.1426.
[31] L.M. Haas, et al., Phys. Rev. D 87 (2013) 076004, arXiv:1302.1993.
[32] K. Fukushima, Phys. Rev. D 77 (2008) 114028, arXiv:0803.3318.
[33] K. Fukushima, Phys. Lett. B 591 (2004) 277, arXiv:hep-ph/0310121.
[34] B. Lucini, A. Rago, E. Rinaldi, Phys. Lett. B 712 (2012) 279, arXiv:1202.6684.
[35] B. Lucini, M. Teper, U. Wenger, J. High Energy Phys. 0401 (2004) 061, arXiv:hep-lat/0307017.
[36] P. de Forcrand, L. von Smekal, Phys. Rev. D 66 (2002) 011504, arXiv:hep-lat/0107018.
[37] M. Le Bellac, Thermal Field Theory, Cambridge University Press, 1996.
[38] D. Toublan, Phys. Lett. B 621 (2005) 145, arXiv:hep-th/0501069.
[39] C. Wetterich, Phys. Lett. B 301 (1993) 90.
[40] J. Berges, N. Tetradis, C. Wetterich, Phys. Rep. 363 (2002) 223, arXiv:hep-ph/0005122.
[41] J. Polonyi, Cent. Eur. J. Phys. 1 (2003) 1, arXiv:hep-th/0110026.
[42] J.M. Pawlowski, Ann. Phys. 322 (2007) 2831, arXiv:hep-th/0512261.
[43] B.J. Schaefer, J. Wambach, Phys. Part. Nucl. 39 (2008) 1025, arXiv:hep-ph/0611191.
[44] H. Gies, Lect. Notes Phys. 852 (2012) 287, arXiv:hep-ph/0611146.
[45] J. Braun, J. Phys. G 39 (2012) 033001, arXiv:1108.4449.
[46] D.F. Litim, Phys. Rev. D 64 (2001) 105007, arXiv:hep-th/0103195.
[47] D.F. Litim, J.M. Pawlowski, J. High Energy Phys. 0611 (2006) 026, arXiv:hep-th/0609122.
[48] J. Braun, K. Schwenzer, H.J. Pirner, Phys. Rev. D 70 (2004) 085016, arXiv:hep-ph/0312277.
[49] A. Pelissetto, E. Vicari, Phys. Rep. 368 (2002) 549, arXiv:cond-mat/0012164.
[50] J. Braun, et al., Phys. Rev. Lett. 106 (2011) 022002, arXiv:0908.0008.